CARBON letters

Original Articles
Carbon Letters Vol. 20, 32-38 (2016)

Morphologies and surface properties of cellulose-based activated carbon nanoplates

Seulbee Lee[1], Min Eui Lee[1], Min Yeong Song[1], Se Youn Cho[1], Young Soo Yun[2] and Hyoung-Joon Jin[1,♠]

[1]Department of Polymer Science and Engineering, Inha University, Incheon 402-751, South Korea
[2]Department of Chemical Engineering, Kangwon National University, Samcheok 245-711, South Korea

Article Info

Received 5 January 2016
Accepted 25 February 2016

♠Corresponding Author
E-mail: hjjin@inha.ac.kr
Tel: +82-32-860-7483

Open Access

DOI: http://dx.doi.org/10.5714/CL.2016.20.032

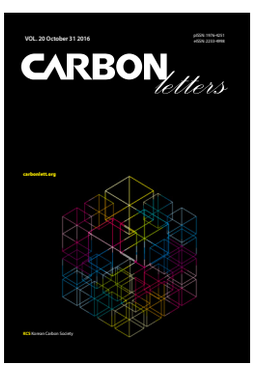

http://carbonlett.org

pISSN: 1976-4251
eISSN: 2233-4998

Abstract

In this study, cellulose nanoplates (CNPs) were fabricated using cellulose nanocrystals obtained from commercial microcrystalline cellulose (MCC). Their pyrolysis behavior and the characteristics of the product carbonaceous materials were investigated. CNPs showed a relatively high char yield when compared with MCC due to sulfate functional groups introduced during the manufacturing process. In addition, pyrolyzed CNPs (CCNPs) showed more effective chemical activation behavior compared with MCC-induced carbonaceous materials. The activated CCNPs exhibited a microporous carbon structure with a high surface area of 1310.6 m^2/g and numerous oxygen heteroatoms. The results of this study show the effects of morphology and the surface properties of cellulose-based nanomaterials on pyrolysis and the activation process.

Key words: cellulose nanocrystals, carbon nanoplates, carbonization, activation, activated carbon

1. Introduction

Two-dimensional (2D) carbon-based nanomaterials (CNMs) such as graphene, carbon nanosheets, and carbon nanoplates have attracted tremendous attention due to their unique properties. These include such as excellent electronic conductivity, high chemical stability, large surface area, and low cost [1-4]. The physical and chemical properties of CNMs are highly dependent on their morphologies, components, and microstructural characteristics. Numerous attempts have been made to prepare and characterize 2D CNMs using diverse carbon precursors and synthesis processes [5-8]. Among the various processes for manufacturing CNMs, pyrolysis of polymeric material has the merits of large scale production, wide availability, and cost effectiveness [9]. Cellulose, a natural polymer composed of anhydro-D-glucopyranose units linked by β-1,4-glycosidic bonds, is a well-known carbon precursor used commonly as a source for carbon fibers. However, the disadvantages of low carbon yield and poor mechanical properties when compared with, polyacrylonitrile-based carbon fibers, has inhibited the production of cellulose-based carbon fibers [10,11]. A combination of increased demand for new CNMs and general environmental awareness has led to a resurgence in the use of cellulosic precursors in recent years [12,13].

Cellulose consists of alternating highly ordered crystalline regions organized by numerous inter-/intra-chain hydrogen bonding between cellulose molecules, and less-ordered amorphous regions. Cellulose nanocrystals (CNs), rod-like nanoparticles with high aspect ratios, are acquired by retaining cellulose nano-fibrils along the transverse direction and disrupting amorphous segments under controlled acid hydrolysis or mechanical force [14-16]. Due to their excellent mechanical properties, chemical tenability, low density, renewability, and low cost, CNs have been primarily investigated for application as reinforcement fillers in polymer nanocomposites [17-20]. In recent years, new attempts have been reported to extend the applications of CNs by fabricating mi-

cro-/nano-structured foams using a freeze drying technique [21-23]. Several materials with different morphology (e.g., porous, cellular, fibrous, and plates) were fabricated using controlled growth and sublimation of ice crystals in a CN suspension (freezing temperature, suspension concentration, atmosphere pressure, cooling rate, and particle size).

In this study, we fabricated cellulose nanoplates (CNPs) using a freeze drying technique and investigated their pyrolysis and activation behaviors. Through comparisons with commercial microcrystalline cellulose (MCC), the pyrolysis behaviors of cellulose-based carbon materials at nanometer-scale were examined. Pyrolyzed CNPs (CCNPs) and activated CCNPs (ACCNPs) showed different morphological or topographic characteristics, and distinct microstructures, when compared to MCC-based carbon materials.

2. Experimental

2.1. Preparation of CNs

MCC (20 μm; Sigma Aldrich, St. Louis, MO, USA) from cotton linter was used as raw material. CNs were prepared via the hydrolysis of MCC using sulfuric acid (H_2SO_4, 95%; OCI Co., Seoul, Korea). Acid hydrolysis was performed at 45°C with 65 wt% H_2SO_4 for 1 h under continuous stirring. After the reaction, the suspension was diluted with 200 mL of distilled water and then centrifuged at 3000 r/min for 15 min to separate the CNs (MR 23i; Jouan, Winchester, VA, USA). The obtained CNs were then dialyzed using tubing cellulose membrane (typical molecular weight cut-off = 14,000; Sigma Aldrich) until reaching neutral pH. The final concentration of the CNs in suspension was approximately 1 wt%.

2.2. Preparation of CNPs

The CNs suspension was gradually frozen in dry ice for 1 h. Once completely frozen, the products were placed in a lyophilizer (ALPHA 1-2 LD plus; Fisher Bioblock Scientific, France), and then freeze dried at –50°C and 0.0045 mbar for 4 d to remove the solvent. Finally, the dried white product was obtained and stored in a vacuum oven at 30°C.

2.3. Pyrolysis of MCC and CNPs

It has been proposed that the pyrolysis of cellulose proceeds in the following four stages: 1) the physical desorption of water (25°C–150°C); 2) dehydration from the cellulose unit (150°C–240°C); 3) thermal cleavage of the glycosidic linkage, with scission of other C-O bonds and some C-C bonds via free-radical reactions (240°C–400°C); and 4) aromatization (400°C and above) [24]. In this study, both MCC and CNPs were initially stabilized at 150°C in air for 2 h. After stabilization, the samples were pyrolyzed to 800°C in a nitrogen atmosphere at a heating rate of 2°C/min, followed by a 2 h isotherm. All heat treatment was performed in a tubular furnace. The resulting carbonaceous samples (Pyrolyzed MCC [CMCC] and CCNPs) were washed with distilled water and ethanol several times and stored in a vacuum oven at 30°C.

2.4. Preparation of activated CMCC and CCNPs

The CMCC and CCNPs were chemically activated with KOH (carbon to KOH ratio of 1:1) (95%, OCI Co.) at 800°C for 2 h at a heating rate of 10°C/min under N_2 gas in a tubular furnace. The resulting samples (activated-CMCC [ACMCC] and -CCNPs [ACCNPs]) were washed with distilled water and ethanol several times; then stored in a vacuum oven at 30°C.

2.5. Characterization

The morphologies of the MCC and CNPs were investigated via field-emission scanning electron microscopy (FE-SEM) (S-4300; Hitachi, Tokyo, Japan) after Pt coating (E-1030; Hitachi). The formation of CNs was examined using atomic force microscopy (AFM) (Multimode IVa; Bruker, Billerica, MA, USA). The pyrolysis behaviors of MCC and CNPs were studied using a thermogravimetric analyzer (TGA) (Q50; TA instruments, West Sussex, UK) from room temperature to 800°C at a heating rate of 5°C/min under N_2 atmosphere. The chemical bonding characteristics of the samples were evaluated via X-ray photoelectron spectroscopy (XPS) (PHI 5700 ESCA; Physical Electronics, Chanhassen, MN, USA) using monochromatic Al-Kα radiation (hv = 1486.6 eV). X-ray diffraction (XRD) (DMAX 2500; Rigaku, Tokyo, Japan) analysis for the carbonaceous materials was carried out using Cu-Kα X-radiation (λ = 0.154 nm) at 40 kV and 100 mA. Raman spectroscopy (Jobin Yvon, Longjumeau, France) was used to determine the microstructure of the samples. The surface area and pore properties of the samples were characterized using the Brunauer-Emmett-Teller method (Tristar 3000; Micromeritics, Norcross, GA, USA).

3. Results and Discussion

3.1. Morphology and surface characteristics of MCC, CNs, and CNPs

Fig. 1a shows a schematic diagram and images of the fabrication of CNPs using CNs. The CNs were prepared using commercial MCC exhibiting irregular shapes, as shown in Fig. 1b. Following sulfuric acid hydrolysis, the formation of rod-like nanoparticles (CNs) with an average length of 170 ± 7 nm and width of 17 ± 5 nm was confirmed via AFM analysis, as revealed in Fig. 1c. These dimensions are similar to the dimensions and aspect ratio (~10) of the cotton-linter based CNs reported elsewhere [25]. The strong acids and mechanical forces resulted in the removal of amorphous segments of pristine cellulose, and accordingly, the bulk MCC broke down into rod-like CNs. During the sulfuric acid treatment, it is known that negatively charged sulfate groups attach to the surface of CNs, limiting hydrogen bonds between the individual CNs via electrostatic repulsive force [26]. As a result, CN dispersion can be stable and homogeneous in an aqueous solution, and the suspended CNs are organized into nanoplate structures by being rejected by the growing ice

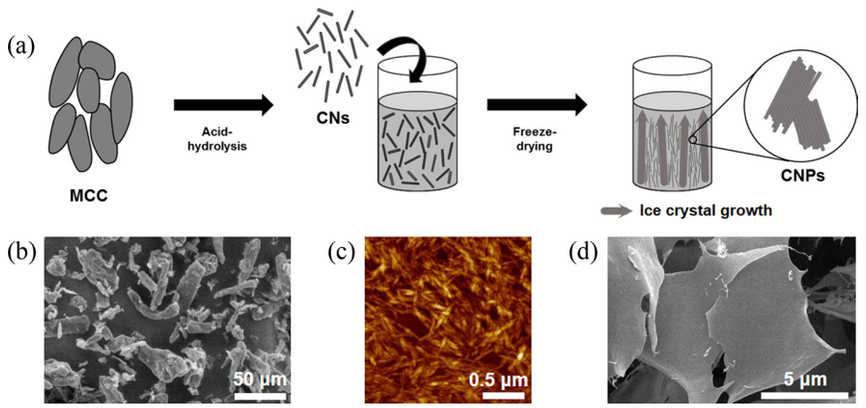

Fig. 1. (a) Schematic diagram of the entire process, including the preparation of cellulose nanoplates (CNPs); (b) field-emission scanning electron microscopy (FE-SEM) image of microcrystalline cellulose (MCC); (c) atomic force microscopy images of cellulose nanocrystals (CNs) after acid hydrolysis reaction, and (d) FE-SEM image of CNPs after the freeze-drying process.

crystal to accumulate in the spaces between the ice crystals [22,27]. After freeze-drying, CNs self-assembled into nanoplate-like structures (CNPs) as shown in Fig. 1d via a template effect from the ice crystals. In addition, the same procedure was carried out using MCC, where no plate-like structures were observed, and the MCCs maintained their initial shapes.

3.2. The pyrolysis behavior of MCC and CNPs

The TGA curves in Fig. 2 show that the pyrolysis behaviors of MCC and CNPs developed through several decomposition stages. By ~100°C, both MCC and CNPs showed a small initial weight loss (approximately 5%) attributed to the evaporation of adsorbed moisture. In case of MCC, a dramatic weight loss at approximately 300°C was observed that resulted from the dehydration and decomposition of cellulose molecules, and is similar to that of pristine cellulose, as reported elsewhere [28]. A char residue of ~13 wt% remained through the aromatization process (above 400°C) from the MCC after pyrolysis at 800°C; however, the CNPs revealed a different pyrolysis behavior than that of the MCC. Even though the thermal decomposition of the CNPs started at a relatively low temperature (~140°C), the yield of CNP char residues (~22%) was significantly higher than that of MCC. Various surface properties induced by strong acid treatment, such as the creation of free-end chains and the introduction of sulfate groups in CNs, might play an important role in diminishing their thermal stability [29,30]. The high yield of CNP char residues can be interpreted as due to the presence of sulfate groups on their surfaces [31]. Sulfate groups may be responsible for solid-gas phase transition catalysis; during the pyrolysis process, sulfate groups expedite the dehydration at lower temperature. Through vigorous thermal motion at temperatures above 140°C, sulfate groups chemically extract water from cellulose and the water would evaporate immediately, as follows:

$$C_n(H_2O)_m \rightarrow mH_2O + nC$$

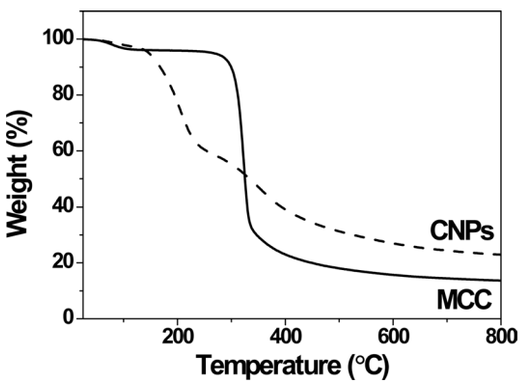

Fig. 2. Thermogravimetric analyzer (5°C/min in N_2) curves of microcrystalline cellulose (MCC, solid line), and cellulose nanoplates (CNPs, dashed line).

Removing oxygen atoms in the form of water would inhibit weight loss and contribute to the increasing char yield by suppressing the release of CO and CO_2, which is related to significant weight loss during the pyrolysis of cellulose.

3.3. Morphologies and microstructures of CMCC, ACMCC, CCNPs, and ACCNPs

The morphologies of CMCC, CCNPs, and their activation products, ACMCC and ACCNPs, were confirmed via FE-SEM, and are revealed in Fig. 3. It was confirmed that both MCC and CNPs maintained their morphologies after pyrolysis and activation. The microstructures of the samples were characterized via XRD. All XRD patterns shown in Fig. 4 exhibited broad peaks centered at approximately $2\theta = 22°–23°$, and 43°–44°, corresponding to the (002) and (100) planes, respectively, of the typical amorphous carbon structure. The peak positions differed slightly from sample to sample. The (002) peak was observed in CMCC at approximately 22.4°, while that in CCNPs was indicated at approximately 23°. These results suggest that the increased crystallinity index affects the rearrangement of crystalline regions into a more

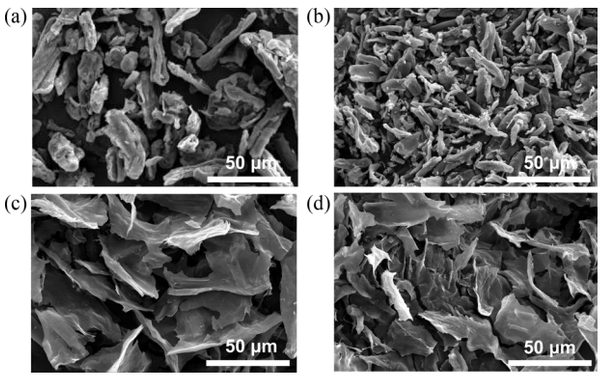

Fig. 3. Field-emission scanning electron microscopy images of cellulose-derived materials: (a) pyrolyzed microcrystalline cellulose (CMCC), (b) activated CMCC (ACMCC), (c) pyrolyzed cellulose nanoplates (CCNPs), and (d) activated CCNPs (ACCNPs).

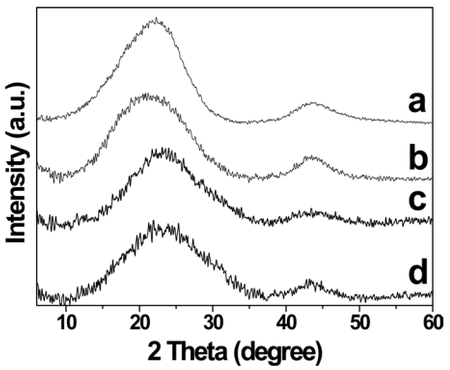

Fig. 4. X-ray diffraction patterns of (a) pyrolyzed microcrystalline cellulose (CMCC), (b) activated CMCC (ACMCC), (c) pyrolyzed cellulose nanoplates (CCNPs), and (d) activated CCNPs (ACCNPs).

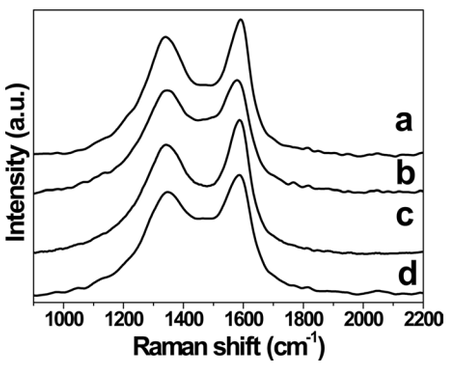

Fig. 5. Raman spectra of (a) pyrolyzed microcrystalline cellulose (CMCC), (b) activated CMCC (ACMCC), (c) pyrolyzed cellulose nanoplates (CCNPs), and (d) activated CCNPs (ACCNPs).

ordered carbon structure [32,33]. Additionally, the XRD patterns of activated carbonaceous materials are shown to shift toward lower angles when compared to non-activated carbonaceous materials, which results from the expansion of CMCC and CCNP carbon lattices via the intercalation/extraction of potassium during the activation process. Further studies of the sample microstructures were carried out via Raman spectroscopy in Fig. 5. The bands centered at ~1355 and ~1582 cm^{-1} in the Raman spectrum are the representative peaks characteristic of hexagonal carbon materials, and correspond to *D* bands (disordered) and *G* bands (ordered), respectively. The *D* bands arise from the breathing mode of sp^2 sites in rings, not in chains; and the *G* bands represent the stretching vibration of any pair of sp^2 sites, whether in C=C chains or in aromatic rings [34]. The extended band range is due to amorphous characteristics with a defective hexagonal carbon structure. Specifically, the ratio of *D* and *G* bands (I_D/I_G) can be regarded as a measure of the structural order of various carbonaceous materials [35]. The intensity ratios for two peaks (I_D/I_G) of CMCC, ACMCC, CCNP, and ACCNP; were 0.87, 0.91, 0.81, and 0.86, respectively. The slightly higher I_D/I_G ratios of the activated carbon materials are reasonable, because they were chemically attacked by an activation agent, inducing a disordered-carbon structure.

3.4. Chemical characteristics of CMCC, ACMCC, CCNPs, and ACCNPs

As shown in Fig. 6, XPS was used to investigate the changes in chemical compositions according to pyrolysis and/or chemical activation of MCC and CNPs. All samples (CMCC, ACMCC, CCNPs, and ACCNPs) were composed primarily of carbon and oxygen atoms, but the C/O ratios differed from sample to sample. Three distinct peaks of the samples were observed in the XPS C 1*s* spectra with binding energies of 284.5, 286.0, and 257.6 eV; corresponding to C-C/C=C, C-O, and C=O, respectively. Two peaks in the O 1*s* region can be confirmed with binding energies of 531.5–532.0 and 533.0 eV, corresponding to C=O and C-O, respectively [36,37]. The individual spectra show changes in the chemical components according to the pyrolysis and activation processes. During the pyrolysis of the cellulose molecules, based on release of CO and/or CO_2, the C=O and C–O–C species were transformed into C-C or C=C. This transformation increased due to dehydration, depolymerization, and aromatization. In addition, the amount of oxygen in the samples increased after chemical activation [38]. More specific C/O ratios can be seen in Table 1.

Table 1. Specific surface area and chemical composition of CMCC, CCNPs, ACMCC, and ACCNPs

Sample	S_{BET} (m^2/g)	C (at%)	O (at%)	C/O
MCC	1.4	57.9	42.1	1.4
CNPs	1.8	56.3	43.7	1.3
CMCC	265.0	89.8	10.2	8.8
CCNPs	384.3	86.2	13.8	6.3
ACMCC	1166.2	88.8	11.2	7.93
ACCNPs	1310.6	83.4	16.6	5.0

CMCC, pyrolyzed MCC; CCNPs, pyrolyzed CNP; ACMCC, activated CMCC; ACCNPs, activated CCNPs; BET, Brunauer-Emmett-Teller; MCC, microcrystalline cellulose; CNPs, cellulose nanoplates.

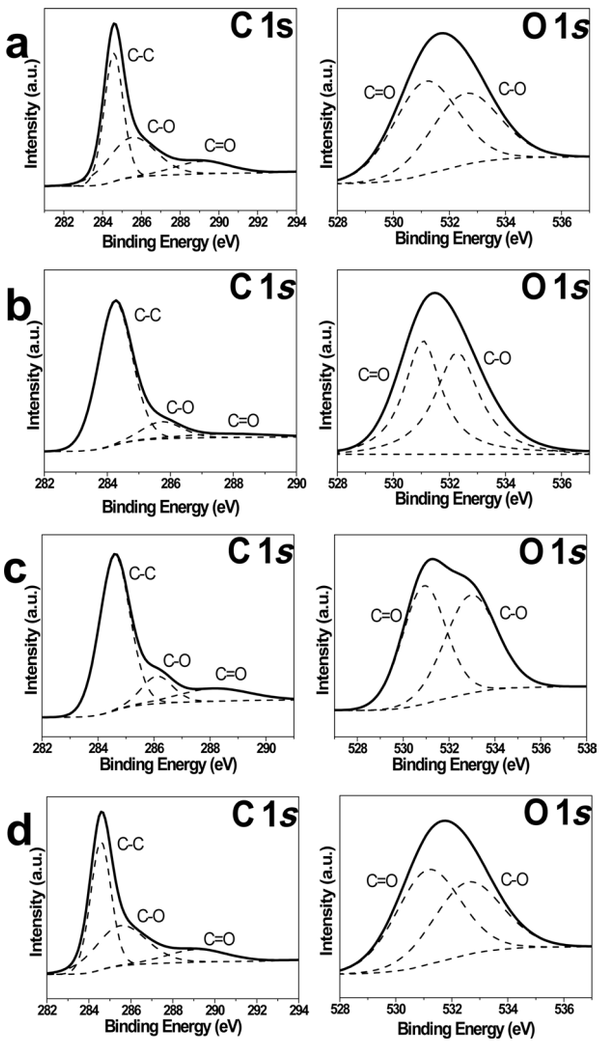

Fig. 6. X-ray photoelectron spectroscopy of C 1*s* and O 1*s* of (a) pyrolyzed microcrystalline cellulose (CMCC), (b) activated CMCC (ACMCC), (c) pyrolyzed cellulose nanoplates (CCNPs), and (d) activated CCNPs (ACCNPs).

3.5. Surface area characteristics of CMCC, CCNPs, ACMCC, and ACCNPs

As shown in Fig. 7, the pore characteristics of the CMCC, ACMCC, CCNPs, and ACCNPs were investigated via nitrogen adsorption/desorption isotherm curves. The isotherm curves related to adsorption/desorption, indicate the specific volume adsorbed on the sample as a function of relative pressure (P/P_0). The isotherm curves of CMCC and CCNPs are of International Union of Pure and Applied Chemistry (IUPAC) type-IV, indicating a mesoporous pore structure [39]. CCNPs show a greater surface area than that of CMCC, which might be induced by the nanostructures of the CNPs. The sulfate groups on the CNP surface can also be utilized as an activation agent [40], leading to more effective activation. However, after the activation process, ACMCC and ACCNPs exhibited typical characteristics of IUPAC type-I isotherm curves, implying the existence of well-developed micropores. Metallic K is produced at temperatures above 700°C in the KOH activation process and intercalates into the carbon lattices, expanding the space between the lattices and increasing the specific surface area [41]. Also, the ACCNPs have a higher surface area than that of ACMCC, suggesting that a more effective activation occurs in CCNPs. Additional details related to the surface area properties of the samples are shown in Table 1.

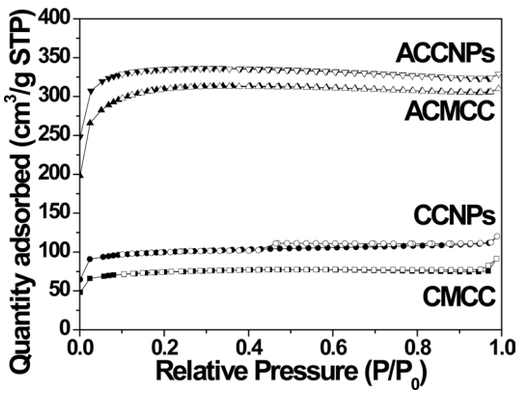

Fig. 7. Adsorption/desorption isotherms of N_2, for different carbonaceous materials. The closed symbols represent adsorption, and the open symbols represent desorption. STP, standard temperature pressure; CCNPs, pyrolyzed cellulose nanoplates; CMCC, pyrolyzed microcrystalline cellulose; ACCNPs, activated CCNPs; ACMCC, activated CMCC.

4. Conclusions

In summary, we fabricated CNPs using CNs via an ice template technique, and investigated the pyrolysis behavior and chemical activation effects with KOH. Strong acid treatment of commercial MCC resulted in the formation of rod-like CNs with an average length and width of 170 ± 7 nm and 17 ± 5 nm, respectively. CNPs prepared from CNs via self-assembly exhibited significantly different pyrolysis behaviors and product materials compared with those of MCC. The pyrolysis of CNPs induced relatively high char-yields due to the free-end chains and the presence of sulfate groups. The CMCC, CCNP, ACMCC, and ACCNP samples exhibited a typical amorphous carbon structure composed of defective hexagonal carbon planes. Chemical activation resulted in carbon structures with a higher defect density. The pyrolyzed and/or activated samples were composed primarily of carbon and oxygen atoms, and the activation process further increased the oxygen content. While the CCNPs and CMCC exhibited a mesoporous carbon structure, the ACCNPs and ACMCC had microporous carbon structures with significantly increased surface areas. In addition, CNP-based samples showed higher surface area than those of the MCC-based samples.

Conflict of Interest

No potential conflict of interest relevant to this article was reported.

Acknowledgements

This research was supported by a grant from the Technology Development Program for Strategic Core Materials funded by the Ministry of Trade, Industry & Energy, Republic of Korea (Project No. 10050858), and by a grant from the Technology Development Program for Industrial Core funded by the Ministry of Trade, Industry & Energy, Republic of Korea (Project No. 10067368).

References

[1] Peres NMR, Guinea F, Neto AHC. Electronic properties of disordered two-dimensional carbon. Phys Rev B, **73**, 125411 (2006). http://dx.doi.org/10.1103/physrevb.73.125411.

[2] Pandolfo AG, Hollenkamp AF. Carbon properties and their role in supercapacitors. J Power Sources, **157**, 11 (2006). http://dx.doi.org/10.1016/j.jpowsour.2006.02.065.

[3] Zhu J, Yang D, Yin Z, Yan Q, Zhang H. Graphene and graphene-based materials for energy storage applications. Small, **10**, 3480 (2014). http://dx.doi.org/10.1002/smll.201303202.

[4] Yun YS, Cho SY, Shim J, Kim BH, Chang SJ, Baek SJ, Huh YS, Tak Y, Park YW, Park S, Jin HJ. Microporous carbon nanoplates from regenerated silk proteins for supercapacitors. Adv Mater, **25**, 1993 (2013). http://dx.doi.org/10.1002/adma.201204692.

[5] Yun YS, Le VD, Kim H, Chang SJ, Baek SJ, Park S, Kim BH, Kim YH, Kang K, Jin HJ. Effects of sulfur doping on graphene-based nanosheets for use as anode materials in lithium-ion batteries. J Power Sources, **262**, 79 (2014). http://dx.doi.org/10.1016/j.jpowsour.2014.03.084.

[6] Xu G, Ding B, Shen L, Nie P, Han J, Zhang X. Sulfur embedded in metal organic framework-derived hierarchically porous carbon nanoplates for high performance lithium–sulfur battery. J Mater Chem A, **1**, 4490 (2013). http://dx.doi.org/10.1039/C3TA00004D.

[7] Wei W, Liang H, Parvez K, Zhuang X, Feng X, Müllen K. Nitrogen-doped carbon nanosheets with size-defined mesopores as highly efficient metal-free catalyst for the oxygen reduction reaction. Angew Chem, **126**, 1596 (2014). http://dx.doi.org/10.1002/ange.201307319.

[8] Yun YS, Park MH, Hong SJ, Lee ME, Park YW, Jin HJ. Hierarchically porous carbon nanosheets from waste coffee grounds for supercapacitors. ACS Appl Mater Interfaces, **7**, 3684 (2015). http://dx.doi.org/10.1021/am5081919.

[9] Hornyak GL, Dutta J, Tibbals HF, Rao A. Introduction to Nanoscience, CRC Press, Boca Raton, (2008).

[10] Huang X. Fabrication and properties of carbon fibers. Materials, **2**, 2369 (2009). http://dx.doi.org/10.3390/ma2042369.

[11] Dumanlı AG, Windle AH. Carbon fibres from cellulosic precursors: a review. J Mater Sci, **47**, 4236 (2012). http://dx.doi.org/10.1007/s10853-011-6081-8.

[12] White RJ. The Search for Functional Porous Carbons from Sustainable Precursors. In: White RJ, ed. Porous Carbon Materials from Sustainable Precursors, RSC Green Chemistry Vol. 32, Royal Society of Chemistry, Cambridge, 3 (2015). http://dx.doi.org/10.1039/9781782622277-00003.

[13] Wei L, Yushin G. Nanostructured activated carbons from natural precursors for electrical double layer capacitors. Nano Energy, **1**, 552 (2012). http://dx.doi.org/10.1016/j.nanoen.2012.05.002.

[14] Bai W, Holbery J, Li K. A technique for production of nanocrystalline cellulose with a narrow size distribution. Cellulose, **16**, 455 (2009). http://dx.doi.org/10.1007/s10570-009-9277-1.

[15] Moon RJ, Martini A, Nairn J, Simonsen J, Youngblood J. Cellulose nanomaterials review: structure, properties and nanocomposites. Chem Soc Rev, **40**, 3941 (2011). http://dx.doi.org/10.1039/c0cs00108b.

[16] Cho SY, Park HH, Yun YS, Jin HJ. Cellulose nanowhisker-incorporated poly(lactic acid) composites for high thermal stability. Fibers Polym, **14**, 1001 (2013). http://dx.doi.org/10.1007/s12221-013-1001-y.

[17] Sanchez-Garcia MD, Lagaron JM. On the use of plant cellulose nanowhiskers to enhance the barrier properties of polylactic acid. Cellulose, **17**, 987 (2010). http://dx.doi.org/10.1007/s10570-010-9430-x.

[18] Pei A, Malho JM, Ruokolainen J, Zhou Q, Berglund LA. Strong nanocomposite reinforcement effects in polyurethane elastomer with low volume fraction of cellulose nanocrystals. Macromolecules, **44**, 4422 (2011). http://dx.doi.org/10.1021/ma200318k.

[19] Liu H, Liu D, Yao F, Wu Q. Fabrication and properties of transparent polymethylmethacrylate/cellulose nanocrystals composites. Bioresour Technol, **101**, 5685 (2010). http://dx.doi.org/10.1016/j.biortech.2010.02.045.

[20] Peresin MS, Habibi Y, Zoppe JO, Pawlak JJ, Rojas OJ. Nanofiber composites of polyvinyl alcohol and cellulose nanocrystals: manufacture and characterization. Biomacromolecules, **11**, 674 (2010). http://dx.doi.org/10.1021/bm901254n.

[21] Dash R, Li Y, Ragauskas AJ. Cellulose nanowhisker foams by freeze casting. Carbohydr Polym, **88**, 789 (2012). http://dx.doi.org/10.1016/j.carbpol.2011.12.035.

[22] Han J, Zhou C, Wu Y, Liu F, Wu Q. Self-assembling behavior of cellulose nanoparticles during freeze-drying: effect of suspension concentration, particle size, crystal structure, and surface charge. Biomacromolecules, **14**, 1529 (2013). http://dx.doi.org/10.1021/bm4001734.

[23] Peng Y, Gardner DJ, Han Y. Drying cellulose nanofibrils: in search of a suitable method. Cellulose, **19**, 91 (2012). http://dx.doi.org/10.1007/s10570-011-9630-z.

[24] Jenkins GM, Kawamura K. Polymeric Carbons-Carbon Fibre, Glass and Char, Cambridge University Press, New York (1976).

[25] Roohani M, Habibi Y, Belgacem NM, Ebrahim G, Karimi AN, Dufresne A. Cellulose whiskers reinforced polyvinyl alcohol copolymers nanocomposites. Eur Polym J, **44**, 2489 (2008). http://dx.doi.org/10.1016/j.eurpolymj.2008.05.024.

[26] Cho SY, Yun YS, Jin H. Carbon nanofibers prepared by the carbonization of self-assembled cellulose nanocrystals. Macromol Res, **22**, 753 (2014). http://dx.doi.org/10.1007/s13233-014-2094-x.

[27] Deville S. Ice-templating, freeze casting: beyond materials processing. J Mater Res, **28**, 2202 (2013). http://dx.doi.org/10.1557/jmr.2013.105.

[28] Yang H, Yan R, Chen H, Lee DH, Zheng C. Characteristics of hemicellulose, cellulose and lignin pyrolysis. Fuel, **86**, 1781 (2007). http://dx.doi.org/10.1016/j.fuel.2006.12.013.

[29] Li W, Yue J, Liu S. Preparation of nanocrystalline cellulose via ultrasound and its reinforcement capability for poly(vinyl alcohol) composites. Ultrason Sonochem, **19**, 479 (2012). http://dx.doi.org/10.1016/j.ultsonch.2011.11.007.

[30] Lu P, Hsieh YL. Preparation and properties of cellulose nanocrys-

tals: rods, spheres, and network. Carbohydr Polym, **82**, 329 (2010). http://dx.doi.org/10.1016/j.carbpol.2010.04.073.

[31] Li W, Wang R, Liu S. Nanocrystalline cellulose prepared from softwood kraft pulp via ultrasonic-assisted acid hydrolysis. Bioresources, **6**, 4271 (2011).

[32] Bondeson D, Mathew A, Oksman K. Optimization of the isolation of nanocrystals from microcrystalline cellulose by acid hydrolysis. Cellulose, **13**, 171 (2006). http://dx.doi.org/10.1007/s10570-006-9061-4.

[33] Rosli NA, Ahmad I, Abdullah I. Isolation and characterization of cellulose nanocrystals from Agave angustifolia fibre. Bioresources, **8**, 1893 (2013).

[34] Reich S, Thomsen C. Raman spectroscopy of graphite. Phil Trans R Soc Lond A, **362**, 2271 (2004). http://dx.doi.org/10.1098/rsta.2004.1454.

[35] Ferrari AC. Raman spectroscopy of graphene and graphite: disorder, electron-phonon coupling, doping and nonadiabatic effects. Solid State Commun, **143**, 47 (2007). http://dx.doi.org/10.1016/j.ssc.2007.03.052.

[36] Rhim YR, Zhang D, Fairbrother DH, Wepasnick KA, Livi KJ, Bodnar RJ, Nagle DC. Changes in electrical and microstructural properties of microcrystalline cellulose as function of carbonization temperature. Carbon, **48**, 1012 (2010). http://dx.doi.org/10.1016/j.carbon.2009.11.020.

[37] Zhang H, Zhu L, Sun R. Structure and properties of cotton fibers modified with titanium sulfate and urea under hydrothermal conditions. J Eng Fiber Fabr, **9**, 67 (2014).

[38] Lee D, Cho S, Kim Y, Lee YS. Influence of the pore properties on carbon dioxide adsorption of PAN-based activated carbon nanofibers. Polymer (Korea), **37**, 592 (2013). http://dx.doi.org/10.7317/pk.2013.37.5.592.

[39] Weidenthaler C. Pitfalls in the characterization of nanoporous and nanosized materials. Nanoscale, **3**, 792 (2011). http://dx.doi.org/10.1039/C0NR00561D.

[40] Sahira J, Mandira A, Prasad PB, Ram PR. Effects of activating agents on the activated carbons prepared from lapsi seed stone. Res J Chem Sci, **3**, 19 (2013).

[41] Miller JR, Outlaw RA, Holloway BC. Graphene double-layer capacitor with ac line-filtering performance. Science, **329**, 1637 (2010). http://dx.doi.org/10.1126/science.1194372.